ARTICLE OPEN

Check for updates

Classification of second harmonic generation effect in magnetically ordered materials

Rui-Chun Xiao[1]✉, Ding-Fu Shao[2], Wei Gan[1], Huan-Wen Wang[3], Hui Han[1], Z. G. Sheng[4], Changjin Zhang[1,4], Hua Jiang[5,6]✉ and Hui Li[1]✉

The relationship between magnetic order and the second harmonic generation (SHG) effect is a fundamental area of study in condensed matter physics with significant practical implications. In order to gain a clearer understanding of this intricate relation, this study presents a comprehensive classification scheme for the SHG effect in magnetically ordered materials. This framework offers a straightforward approach to connecting magnetic order and the SHG effect. The characteristics of the SHG tensors in all magnetic point groups are studied using the isomorphic group method, followed by a comprehensive SHG effect classification scheme that includes seven types based on the symmetries of the magnetic phases and their corresponding parent phases. In addition, a tensor dictionary containing the SHG and linear magneto-optic (LMO) effect is established. Furthermore, an extensive SHG database of magnetically ordered materials is also built up. This classification strategy exposes an anomalous SHG effect with even characteristics (i.e., invariant) under time-reversal symmetry, which is solely contributed by magnetic structure. Moreover, the proposed classification scheme facilitates the determination of magnetic structures through the SHG effect.

npj Quantum Materials (2023)8:62 ; https://doi.org/10.1038/s41535-023-00594-3

INTRODUCTION

Symmetry plays a crucial role in determining the physical properties of matter. In magnetically ordered materials (such as ferromagnetic (FM) materials, antiferromagnetic (AFM) materials, ferrimagnetic materials, etc.), the spin directions of electrons are arranged in orderly fashions, leading to spontaneous time-reversal symmetry breaking and rich physical phenomena. To reveal the symmetries of magnetically ordered materials, optical techniques are usually considered as an effective approach[1–3]. The linear magneto-optic (LMO) effect (refers specifically to the Faraday effect[4] in transmission and Kerr effect[5] in reflection here) and the second harmonic generation (SHG) effect are two basic and complemental optical tools to study magnetic structures in experiments. The SHG effect is particularly powerful in characterizing AFM materials where the LMO method fails, particularly in recent two-dimensional (2D) AFM materials, for example, bilayer CrI_3[6], $MnPS_3$[7], $MnPSe_3$[8], $CrSBr$[9], and NiI_2[10]. Therefore, the SHG effect is widely adopted to detect magnetic phase transitions[11–15], magnetic symmetries, magnetic orders[16–18], and domain structures[13,14,19], due to its spectral and spatial resolution. Therefore, bridging the connection between the SHG effect and magnetic order is a frontier area in this field[12,13].

Comprehensively classifying the SHG effect in magnetically ordered materials offers a promising approach to better understanding the intriguing relationship between the SHG effect and the magnetic structures. However, achieving this goal is still elusive. It is well-known that the appearance of the SHG effect may indicate the breaking of inversion symmetry under the electric dipole approximation. In magnetically ordered materials, the inversion-symmetry-breaking can be induced by either asymmetric crystal structures (inversion symmetry breaking resulting from the parent crystallographic structures) or magnetic structures[20–26]. Birss, in the 1960s[27,28], divided SHG tensors into two types based on their parities under time-reversal symmetry: *i*-type (even with time-reversal symmetry *T*) and *c*-type (odd with time-reversal symmetry *T*). Until now, this two-category classification is widely used[6–9,11,12]. However, the classification faces daunting challenges in distinguishing whether the inversion symmetry is broken. Furthermore, the SHG classification is not mutually exclusive, and spatial symmetry is not considered, leading to the complexity in characterizing the SHG effect. Moreover, the nonsystematic study of all magnetic groups may lead to some misconceptions. For example, the SHG effects in magnetically ordered materials are assumed to be odd with time-reversal symmetry[6–10], since the magnetic structure is reversed under the time-reversal operator. However, it should be noted that even SHG tensor can also be induced by magnetic order individually because no symmetry prohibits it, and this anomalous SHG effect has not been realized in previous literature. Therefore, a comprehensive SHG classification that reveals the characteristics of the SHG effect and accurately identifies the origin of the inversion symmetry breaking, whether it arises from crystallographic or magnetic structures is highly desirable.

In this study, we introduce an SHG classification method in magnetically ordered materials containing these two essential aspects: the SHG characteristics and the origin of the inversion symmetry breaking. Firstly, we use the *isomorphic group method* to transform the SHG tensor under the magnetic point groups into nonmagnetic point groups, thereby revealing the rules governing the SHG tensor. Based on this, we classify the SHG effect into seven types based on the symmetries of the magnetic phases and parent phases. Additionally, we build up a tensor dictionary containing the SHG and LMO effects and establish a comprehensive classification for the magnetically ordered materials in the

[1]Institute of Physical Science and Information Technology, Anhui University, 230601 Hefei, China. [2]Key Laboratory of Materials Physics, Institute of Solid State Physics, Chinese Academy of Sciences, 230031 Hefei, China. [3]School of Physics, University of Electronic Science and Technology of China, 610054 Chengdu, China. [4]High Magnetic Field Laboratory, Chinese Academy of Sciences, 230031 Hefei, China. [5]Institute for Advanced Study, Soochow University, 215006 Suzhou, China. [6]Institute for Nanoelectronic Devices and Quantum Computing, Fudan University, 200433 Shanghai, China. ✉email: xiaoruichun@ahu.edu.cn; jianghuaphy@suda.edu.cn; huili@ahu.edu.cn

MAGNDATA database[29]. Furthermore, our classification strategy predicts an anomalous SHG effect, which exhibits even characteristics with time-reversal symmetry and is contributed by magnetic structure solely. The first-principles calculations on some representative magnetically ordered materials confirm the effectiveness of the proposed classification.

RESULTS

Characteristics of SHG tensors of all magnetic points groups with isomorphic group method

Typically, SHG susceptibility tensors can be divided into *T*-even (*i*-type, χ_{ijk}^{even}) and *T*-odd (*c*-type, χ_{ijk}^{odd}) parts[27,28],

$$\chi_{ijk}^{(2)} = \chi_{ijk}^{\text{even}} + \chi_{ijk}^{\text{odd}}. \tag{1}$$

The subscript *i* (*j* and *k*) denotes the direction of second-order polarization (fundamental incident) of light. The notation of the SHG tensor is presented in Supplementary Notes 1.1 and 3.2.

According to Neumann's principle[27,30–32], the SHG tensors are constrained by the magnetic point groups (MPGs, denoted as M_0) rather than the magnetic space groups (MSGs, denoted as *M*, also known as Shubnikov groups)[33–35]. The point group operations in MPGs contain two categories: the unitary point operators *R*, which do not involve the time operation, such as rotation operation *n* and rotation-inversion operation $\overline{n}$ ($n = 1, 2, 3, 4, 6$), and the anti-unitary point operation R'. The relationship between *R* and R' is described as $R' = TR$, where *T* is the time-reversal symmetry. The MPGs can be divided into three classes based on the presence of the *R* and R': (a) original MPGs, which are constituted by ordinary point groups G_0 and lack any anti-unitary operators R', i.e., $M_0 = G_0$, (b) gray MPGs, in the form of $M_0 = G_0 + TG_0 = G_0 + 1'G_0$ ($1' = 1T$ also means the *T* symmetry), (c) black-white (BW) MPGs $M_0 = S_0 + T(G_0 - S_0) = S_0 + R'S_0$, where S_0 is a halving subgroup of G_0. A brief introduction to MPGs and MSGs is provided in Supplementary Note 1.2.

The transformations of the even and odd SHG tensors under a unitary point operation *R* can be expressed as follows:

$$R : \chi_{ijk}^{\text{even/odd}} = \sum_{lmn} R_{il}R_{jm}R_{kn}\chi_{lmn}^{\text{even/odd}}, \tag{2}$$

where R_{ij} represents an element of the 3×3 matrix for the unitary point operation *R*. According to. Eq. (2), the transformations of the even and odd SHG tensors, i.e., χ_{ijk}^{even} and χ_{ijk}^{odd}, are identical under *R*, since *R* does not contain the time-reversal operation *T*. However, the signs of χ_{ijk}^{even} and χ_{ijk}^{odd} are opposite under the transformations of the anti-unitary point operation R':

$$R' : \chi_{ijk}^{\text{even/odd}} = \pm \sum_{lmn} R_{il}R_{jm}R_{kn}\chi_{lmn}^{\text{even/odd}}. \tag{3}$$

The plus and minus sign in Eq. (3) correspond to the even part (χ_{ijk}^{even}) and the odd part (χ_{ijk}^{odd}) of SHG tensors, respectively[31].

Generally, the characteristics of SHG tensors under all MPGs can be directly obtained by solving the above linear algebra equations with the aid of invariant theory (see refs. [27,30,31] and "Bilbao Crystallographic Server/MTENSOR" website). However, the SHG tensor characteristics in magnetically ordered materials are more complicated than those of non-magnetically ordered materials. Currently, the relationships between MPGs and SHG tensors as well as the rules governing the SHG effect under all MPGs have not been clearly established. This lack of understanding hinders the study of the SHG effect.

Here, we investigate the SHG tensors using the *isomorphic group method*. In group theory, -1 is equivalent to the inversion operator *I*, because $-1 = -(I_0)_{3\times3}$ (I_0 is the identity matrix) and $-I_0$ is the matrix of the inversion operation. Therefore, the transformation of χ_{ijk}^{odd} in Eq. (3) under the anti-unitary point operation R' can be re-written as follows:

$$\begin{aligned} R' : \chi_{ijk}^{\text{odd}} &= -\sum_{lmn} R_{il}R_{jm}R_{kn}\chi_{lmn}^{\text{odd}} \\ &= \sum_{lmn} (-R)_{il}(-R)_{jm}(-R)_{kn}\chi_{lmn}^{\text{odd}} \\ &= \sum_{lmn} (IR)_{il}(IR)_{jm}(IR)_{kn}\chi_{lmn}^{\text{odd}}. \end{aligned} \tag{4}$$

The above equation implies that the constraint imposed by the anti-unitary point operation R' on χ_{ijk}^{odd} is equivalent to an unitary point operation *R* times an inversion operation *I*, i.e., *IR*.

The set of all the unitary *R* and anti-unitary R' operations in a specific magnetically ordered material constitute a closed MPG. The transformations of χ_{ijk}^{odd} under all the unitary point operations *R* ($R \in S_0$) and anti-unitary point operations R' ($R' \in R'S_0$) of a BW MPG M_0 are equivalent to S_0 and IRS_0, respectively. Thus, the symmetry restrictions imposed by a BW MPG M_0 on χ_{ijk}^{odd} is equivalent to a nonmagnetic point group (PG) G_1 ($= S_0 + IRS_0$). Similarly, the symmetry constraint of χ_{ijk}^{even} imposed by a BW MPG M_0 is equivalent to a nonmagnetic PG G_0 ($= S_0 + RS_0$), because the transformations of χ_{ijk}^{even} under *R* and R' are identical, as indicated in Eq. (2) and Eq. (3). Because M_0, G_0, and G_1 are *isomorphic groups*, this implies the isomorphic group method can be employed to transform the SHG tensor under MPGs into nonmagnetic PGs. The SHG tensors of gray and original MPGs can also be obtained using the above isomorphic group method, which is given in Supplementary Note 1.3.

As depicted in Fig. 1, we utilize two nonmagnetic isomorphic PGs, G_0, and G_1, to determine the characteristics of the even (χ_{ijk}^{even}) and odd (χ_{ijk}^{odd}) SHG tensor elements under a BW MPG M_0, respectively. No additional numerical calculations are needed since the characteristics of the SHG tensors of all the nonmagnetic PGs can be found in general nonlinear optics textbooks[36,37]. Importantly, the isomorphic group method elucidates the rules governing the SHG tensors[27,30,31].

The characteristics of the LMO effect in all MPGs are also studied in Supplementary Note 2. In our work, the LMO effect specifically refers to the Faraday effect[4] and Kerr effect[5], both of which belong to linear optics. These two kinds of LMO effects arise from the magneto-circular dichroism in transmission (Faraday effect) or reflectivity (Kerr effect) of polarized light in magnetically ordered materials. It was once believed that the LMO effect could only exist in magnetically ordered materials with nonzero net magnetization. However, with the permitted symmetries, the LMO effect has been theoretically predicted or experimentally observed in AFM materials without net magnetization[38]. Specific examples include collinear AFM materials (such as RuO_2[39–41] and MnTe[42]), coplanar but non-collinear AFM materials (such as Mn_3X (X=Rh, Ir, Pt)[43], Mn_3Y (Y=Ge, Ga, Sn)[44–46] and Mn_3ZN (Z=Ga, Zn, Ag, Ni)[47]), as well as in non-coplanar AFM materials (such as γ-$Fe_{0.5}Mn_{0.5}$[48] and $K_{0.5}RhO_2$[48]). In all, the LMO effect can exist in magnetically ordered materials with permitted MPGs. The higher order magneto-optic effects, such as spontaneous nonreciprocal optical effect[49–52] and the magneto-birefringence effect[53] (Voigt effect[54] and Cotton-Mouton effect[55]), are not investigated in our work.

As stated in the introduction, the LMO and SHG effects are two complementary optical methods to study magnetically ordered materials. The characteristics of SHG and LMO effects in all MPGs are listed in Supplementary Note 3, which provides a dictionary for characterizing the magnetic structures with these two optical techniques in experiments. Moreover, this isomorphic group method is also suitable for other tensors in magnetic systems, such as circular photo-galvanic effect (CPGE) whose susceptibilities comprise 3×3 pseudo-tensors (see Supplementary Note 4 for detail). This indicates that this method is a powerful tool for studying the tensors in magnetic systems.

According to our symmetry analysis, the SHG tensors in all MPGs can be divided into four cases based on their characteristics: (1) original MPGs without inversion symmetry, (2) gray MPGs without inversion symmetry, (3) BW MPGs without inversion symmetry but with *PT* symmetry (combination of time-reversal *T* and spatial inversion *P* symmetry), and (4) BW MPGs without inversion symmetry nor *PT* symmetry. The MPGs and the corresponding SHG characteristics are listed in Table 1. Only the even SHG tensors exist in gray MPGs (Case 2). Only the odd SHG tensor exists in BW MPGs with *PT* symmetry (Case 3). In original MPGs without inversion symmetry (Case 1) and BW MPGs without *P* or *PT* symmetry (Case 4), both the odd and even SHG tensors exist. χ_{ijk}^{even} and χ_{ijk}^{odd} are the same in Case 1. However, χ_{ijk}^{even} and χ_{ijk}^{odd} differ in Case 4 as they are constrained by different isomorphic PGs (G_0 and G_1). Table 1 provides a clear and concise summary of the SHG behavior for different MPGs, which reveals the rules governing the SHG effect under all MPGs.

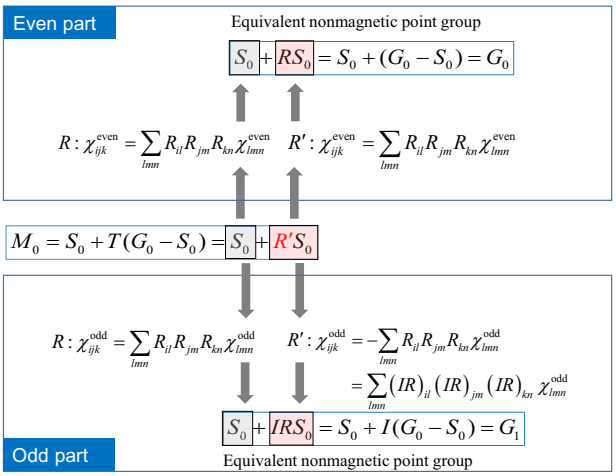

Fig. 1 Diagram of the isomorphic group method to analyze the characteristic of SHG tensor. The transformations of χ_{ijk}^{even} and χ_{ijk}^{odd} under a BW MPG M_0 ($= S_0 + R'S_0$) are equivalent to those under nonmagnetic PGs G_0 ($= S_0 + RS_0$, top panel) and G_1 ($= S_0 + IRS_0$, bottom panel), respectively. S_0 is a halving subgroup of MPG M_0. R is a unitary point operation, R' is an anti-unitary point operation, and I is the inversion operation. Further information is available in Supplementary Note 1.

Classification of the SHG effect in magnetically ordered materials

Next, we classify the SHG effect in magnetically ordered materials based on the symmetries of magnetic and parent structures to reveal the characteristics of the SHG effect further. In view of the fact that breaking the inversion symmetry could arise from either crystallographic or magnetic structure, we should also take the symmetry of the parent phase into account in addition to the magnetic phase, similar to the classification in species of ferromagnetic, ferroelectric, and ferroelastic crystals[56]. In magnetically ordered materials, the parent phases usually exhibit higher symmetry than the magnetic phases. As a consequence, the inversion symmetry broken in the magnetic phases could still be retained in the parent phases. Therefore, each case in Table 1 could be further divided into two subcases, depending on whether parent phases possess inversion symmetry (wP, i.e., with inversion symmetry) or not (woP, i.e., without inversion symmetry). An exception arises in Case 3, as the parent phases must possess the inversion symmetry *P* if the MPGs exhibit *PT* symmetry. Figure 2 depicts the flow chart of the SHG classification scheme. Table 2 presents the seven types of SHG effect, labeled as O-wP, O-woP, G-wP, G-woP, PT-wP, BW-wP, and BW-woP, along with their corresponding characteristics. Because of encompasses all possible SHG cases in magnetically ordered materials, this classification is exhaustive and mutually exclusive.

Figure 2 and Table 2 present a straightforward but practical classification approach. Additionally, the outcomes presented in Table 2 offer valuable insights into the distinct roles of magnetic structures and crystallographic structures in the SHG effect. In other words, this classification strategy reveals the symmetries (containing crystallographic and magnetic symmetries) and physical mechanisms underlying the SHG effect in magnetically ordered materials. For example, magnetically ordered materials with inversion symmetry in their parent phases exhibit four distinctive types of SHG effects, namely, O-wP, G-wP, PT-wP, and BW-wP. All these types of SHG effects arise from magnetic structure rather than crystal asymmetry. In particular, the G-wP type SHG effect is solely contributed by magnetic structures, and only the even SHG tensors are present, which has not yet been explored before. In contrast, only three possible SHG types are anticipated in magnetically ordered materials without inversion symmetry in their parent phases, namely O-woP, G-woP, and BW-woP. The even SHG tensors of these three SHG types arise from crystal and magnetic structures, while the odd SHG tensors solely originate from magnetic structures. This comprehensive classification is superior to the two-category classification (*c*-type and *i*-

Table 1. Characteristics of SHG tensors in all MPGs without inversion symmetry.

SHG cases	Even SHG tensor[a]	Odd SHG tensor	MPGs
Case 1. Original MPG without *P* (20)[b]	✓ $\chi_{ijk}^{\text{even}}(G_0)$ Same as odd	✓ $\chi_{ijk}^{\text{odd}}(G_0)$ Same as even	1(M[c]), 2(M), *m*(M), 222, *mm*2, 4(M), $\bar{4}$(M), 422, 4*mm*, $\bar{4}$2*m*, 3(M), 32, 3*m*, 6(M), $\bar{6}$(M), 622, 6*mm*, $\bar{6}$*m*2, 23, $\bar{4}$3*m*
Case 2. Gray MPG without *P* (20)	✓ $\chi_{ijk}^{\text{even}}(G_0)$	×	11′, 21′, *m*1′, 2221′, *mm*21′, 41′, $\bar{4}$1′, 4221′, 4*mm*1′, $\bar{4}$2*m*1′, 31′, 321′, 3*m*1′, 61′, $\bar{6}$1′, 6221′, 6*mm*1′, $\bar{6}$*m*21′, 231′, $\bar{4}$3*m*1′
Case 3. BW MPG without *P* but with *PT* (20)	×	✓ $\chi_{ijk}^{\text{odd}}(S_0)$	$\bar{1}'$, 2′/*m*, 2/*m*′, *m*′*m*′*m*′, *mmm*′, 4/*m*′, 4′/*m*′, 4/*m*′*mm*, 4′/*m*′*m*′*m*, 4/*m*′*m*′*m*′, $\bar{3}'$, $\bar{3}'$*m*, $\bar{3}'$*m*′, 6′/*m*, 6/*m*′, 6/*m*′*mm*, 6′/*mmm*′, 6/*m*′*m*′*m*′, *m*′$\bar{3}'$, *m*′$\bar{3}'$*m*
Case 4. BW MPG without *P* nor *PT* (27)	✓ $\chi_{ijk}^{\text{even}}(G_0)$ Different with odd	✓ $\chi_{ijk}^{\text{odd}}(G_1)$ Different with even	2′(M), *m*′ (M), 2′2′2(M), *m*′*m*′2 (M), *m*′*m*2′ (M), 4′, $\bar{4}'$, 4′22′, 42′2′(M), 4′*m*′*m*, 4*m*′*m*′(M), $\bar{4}'$2′*m*, $\bar{4}'$2*m*′, $\bar{4}$2′*m*′(M), 32′(M), 3*m*′(M), 6′, $\bar{6}'$, 6′22′, 62′2′(M), 6′*mm*′, 6*m*′*m*′(M), $\bar{6}'$*m*′2, $\bar{6}'$*m*2′, $\bar{6}$*m*′2′(M), 4′32′, $\bar{4}'$3*m*′

[a]The corresponding SHG tensors are presented in Supplementary Note 3.
[b]The numbers in the first column represent the number of MPGs exhibiting the SHG effect.
[c]The letter "M" in the bracket of the fourth column indicates the MPG permitting the LMO effect.

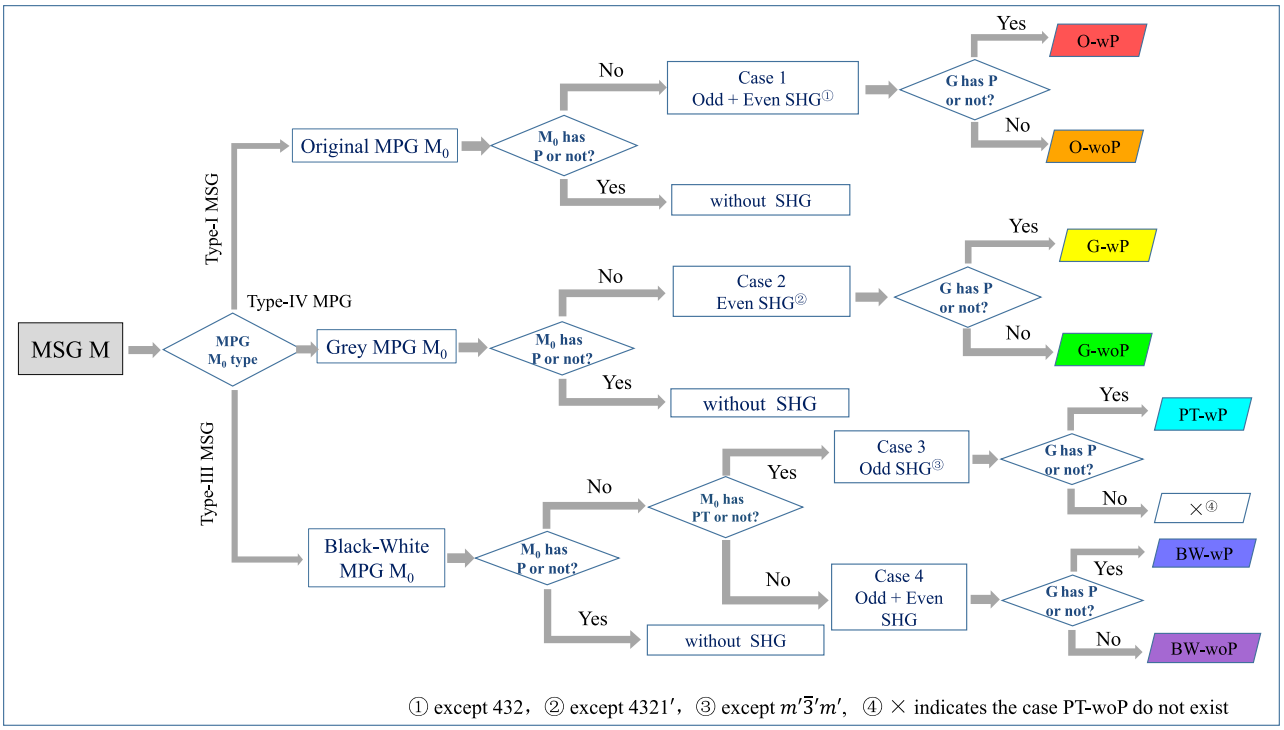

Fig. 2 Flow chart for SHG classification scheme in magnetically ordered materials. First, the MPGs are determined from the MSGs of magnetically ordered materials. Then, the SHG tensors are further divided into four cases based on the symmetries of MPGs (refer to Table 1). Finally, the types of SHG effect in magnetically ordered materials are determined based on whether the parent phases possess inversion symmetry (wP) or not (woP). In this notation, *M* represents the MSG, and *G* in the last judging rhombus denotes the space group (SG) of the parent phase. The colored parallelograms on the right indicate the types of SHG effects. The letter "G" in G-wP and G-woP denotes the gray MPG, and the letter "O" in O-wP and O-woP represents the original MPG. Similarly, "BW" in BW-wP and BW-woP represent the BW MPG without *PT* symmetry, and "PT" in PT-wP indicates the BW MPG with *PT* symmetry. Note that MPGs of 432, 4321′ and $m'\bar{3}'m'$ are excluded because their symmetries forbid the emergence of the SHG effect, even though inversion symmetry is broken.

type)[27,28], since it provides a clearer understanding of the relationship between symmetry and SHG effect.

Now we apply this classification method to real materials. MAGNDATA[29] in the Bilbao Crystallographic Server (BCS) is a well-known material database that encompasses over 1795 magnetic structures. It is worth noting that we refer them to magnetic structures, since one material may possess several magnetic structures. After excluding the incommensurate magnetic structures (the magnetic lattice constants are not integer multiples of those of parent phases)[57], there are 1655 magnetic structures remaining with BCS-ID (identity number in MAGNDATA of BCS) ranging from 0.1–0.835, 1.0.1–1.0.52, 1.1–1.663, 2.1–2.86 and 3.1–3.19. The corresponding materials are listed in Supplementary Table XI. After removing duplicate data, there are 1432 magnetic structures left. Using the process presented in Fig. 2, the SHG effect of each magnetic structure can be classified, as shown in Fig. 3. We find that 496 magnetic structures process the SHG effect, and 451 magnetic structures exhibit the LMO effect. Out of the 496 magnetic structures with the SHG effect, 100 of them also have the LMO effect. The 496 magnetic structures with SHG effect can be further categorized into the above seven types, as illustrated in Fig. 3b. The clarification of the SHG and LMO effects for all magnetic structures in MAGNDATA is compiled into a database which is presented in Supplementary Note 6.

Guided by this classification, we will discuss two examples to validate our isomorphic theory and classification method. The first one involves VBr_2, which suggests that the magnetic structure can induce the even-time-reversal SHG tensors individually. In the second example, we will study the SHG effect in AFM materials $RMnO_3$ (R=Sc, Y, In, Dy, Ho, Er, Tm, Yb, and Lu) with diverse magnetic structures.

Example 1. Anomalous SHG effect in bulk VBr_2

It was previously presumed that the SHG effect induced by magnetic structure would reverse upon switching the magnetic order due to the inherent oddness of magnetic order under time-reversal symmetry. Here, we present a typical example of violating such an assumption in bulk VBr_2[58–60]. As depicted in Fig. 4a, the parent phase of bulk VBr_2 processes the inversion symmetry (SG: $P\bar{3}m1$), and one V atom has six nearest V atoms forming equilateral triangles. Therefore, in-plane geometrical frustration is expected accompanied by the inversion symmetry breaking when the magnetic interactions are antiferromagnetic, as illustrated in Fig. 4b. Additionally, the magnetic moments of the adjacent interlayer V atom are opposite to each other, resulting in the two adjacent layers connected by $T\mathbf{c}/2$ symmetry. Its MSG is P_C31c (P_C means the BW Bravais lattices), as presented in Fig. 4b. According to the classification rule, the SHG type of bulk VBr_2 is classified as G-wP, which is induced by the magnetic structure and it is even under time-reversal symmetry.

The band structures of bulk VBr_2 are shown in Fig. 4c. The bands split because of the breaking inversion symmetry and *PT* symmetry, and the band energies of $+\mathbf{k}$ and $-\mathbf{k}$ points are equivalent due to the "effective" time-reversal symmetry, as shown in the inset of Fig. 4c. The nonzero even components of SHG tensor are constrained by 31*m* symmetry, which means the independent elements are χ^{even}_{xxx} $(=-\chi^{even}_{xyy}=-\chi^{even}_{yxy})$, χ^{even}_{xxz} $(=\chi^{even}_{yyz})$, χ^{even}_{zxx} $(=\chi^{even}_{zyy})$ and χ^{even}_{zzz}. The calculated SHG results are presented in Fig. 4d, which are consistent with the above symmetry analysis. Furthermore, the SHG effect is even with time-reversal symmetry, meaning that reversing the magnetic

Table 2. Classification of the SHG effect based on the symmetries of magnetic structures (i.e., MPGs and MSGs) and parent structures (i.e., parent SGs).

Parent SGs → MPGs / MSGs ↓[a,b]	With inversion symmetry (wP)	Without inversion symmetry (woP)
Case 1. Original MPGs (O) without inversion symmetry (Type-I MSGs)	O-wP Even/odd: from magnetic structure	O-woP Even: from magnetic structure + crystal asymmetry[c] Odd: from magnetic structure
Case 2. Gray MPGs (G) without inversion symmetry (Type-IV MSGs)	G-wP Even: from magnetic structure	G-woP Even: from magnetic structure + crystal asymmetry
Case 3. BW MPGs with *PT* symmetry (PT) (Type-III MSGs)	PT-wP Odd: from magnetic structure	× Not possible
Case 4. BW MPGs without *PT* nor *P* symmetry (BW) (Type-III MSGs)	BW-wP Even/odd: from magnetic structure	BW-woP Even: from magnetic structure + crystal asymmetry Odd: from magnetic structure

[a]A brief introduction to MPGs and MSGs is provided in Supplementary Note 1.2.
[b]The type-II MSGs describe the non-magnetically ordered materials with time-reversal symmetry, which are beyond the scope of our study, and therefore are not included.
[c]"Crystal asymmetry" refers to inversion symmetry breaking resulting from the parent crystal structure.

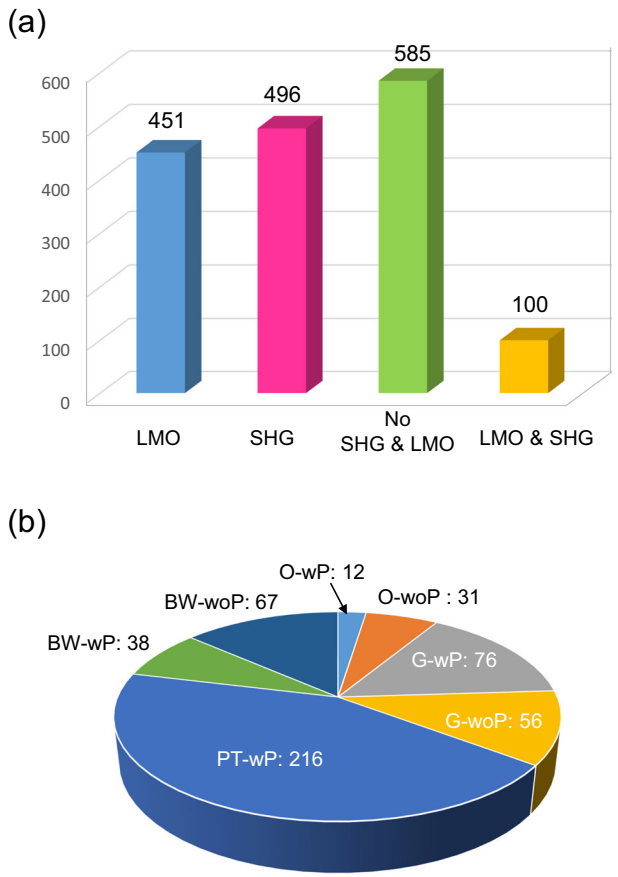

Fig. 3 Statistics on the SHG types in the MAGNDATA database. **a** Counting of materials with SHG and LMO effects in the 1432 magnetic structures (removing duplicate data). **b** Classification of the 496 magnetic structures with SHG effect. The detailed information of every material is presented in Supplementary Note 6.

order does not lead to the reversion of SHG susceptibilities [Fig. 4d].

The G-wP type SHG effect originates from the magnetic structures, and it is even with time-reversal symmetry. These two characteristics are the distinctive features of the G-wP type SHG effect. The anomalous SHG effect in bulk VBr_2 refreshes the conventional understanding that magnetism can only contribute to the odd SHG tensors. In addition, the G-wP type SHG effect is not unusual in real materials, as 76 magnetic structures in the MAGADATA database are proposed to exhibit G-wP SHG effect (Fig. 3b). Therefore, the classification method is a powerful tool for exploring exotic SHG phenomena in magnetically ordered materials.

If the magnetic moments of V atoms in the adjacent interlayers are parallel aligned, as exhibited in the inset of Fig. 4e, the MSG of this magnetic structure is $P31m'$. This magnetic structure leads to the BW-wP type SHG effect according to Fig. 2. The even and odd SHG tensors coexist, and both originate from magnetic structures. The even SHG susceptibilities are basically the same as those in Fig. 4d, and the odd parts are shown in Fig. 4e. We further investigate the SHG effect of bilayer VBr_2 with A-type AFM magnetism, as depicted in Fig. 4f. Due to *PT* symmetry, its bands are doubly degenerate, and the band energies of $+\mathbf{k}$ and $-\mathbf{k}$ points are not equivalent (as illustrated in the inset of Fig. 4g). Since its MSG is $P\bar{3}'m'1$, the corresponding SHG effect belongs to the PT-wP type. Its SHG tensor has only the odd part, and the SHG tensor is constrained by the 32 (D_3) symmetry. The calculated SHG coefficients are shown in Fig. 4h, which are consistent with our symmetry analysis. Indeed, the SHG effect in bilayer VBr_2 with A-type AFM magnetism reverses with the magnetic order, similar to that of bilayer CrI_3[25,61].

Example 2. SHG effect of $RMnO_3$ with various magnetic structures

The parent phase of $RMnO_3$ (R = Sc, Y, In, Dy, Ho, Er, Tm, Yb, and Lu) usually adopts the non-centrosymmetric structure with SG $P6_3cm$, as presented in Fig. 5a. The magnetism primarily arises from the Mn^{3+}, forming approximately equilateral triangles, as illustrated in the bottom panel of Fig. 5b. Below the Néel temperature, the strong super-exchange leads to 120° arrangement of the spins of Mn^{3+} in the basal plane, and small displacements of Mn^{3+} ions (occupy 6*c* positions, see Supplementary Table VIII) break the triangular frustration.

According to the MAGNDATA database and refs. [11,16,17,17,62–65], $RMnO_3$ can exhibit various magnetic structures, such as A_1, A_2, B_1, and B_2 phase presented in Fig. 5b–e. For a specific hexagonal manganite, the ground magnetic order always belongs to one of these states but can be manipulated among them under certain conditions. The pioneering works by Fiebig et al.[16,17,62–65] have proven the SHG effect is a powerful tool for investigating the magnetic structures of $RMnO_3$. In this section, we aim to further

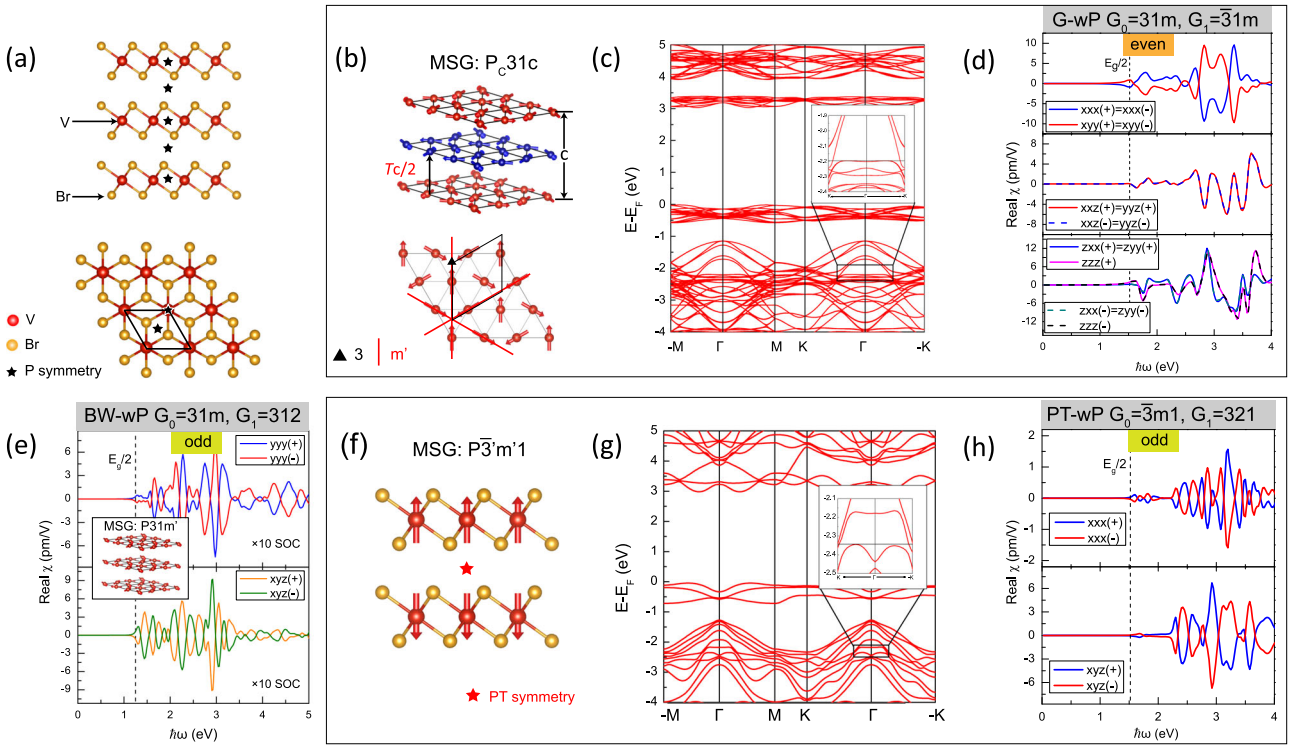

Fig. 4 Calculation results of VBr_2. **a** Crystal structure of the parent phase of bulk VBr_2 (upper panel: side view, lower panel: top view). **b** Magnetic structure (upper panel: side view, lower panel: top view), **c** band structures and **d** nonzero SHG susceptibilities of in-plane frustrated bulk VBr_2. **e** The odd SHG susceptibilities of bulk VBr_2 whose interlayer magnetic moments are parallel aligned. The SOC strength is increased by an order of magnitude to make the odd part of SHG susceptibilities more significant. **f** Magnetic structure (side view), **g** band structures and **h** nonzero SHG susceptibilities of bilayer VBr_2 with A-type AFM magnetic structure. The black rhombuses in **a** and **b** mean the unit cell and magnetic unit cell, respectively. The "+" and " − " signs in **d**, **e**, and **h** denote the positive and negative magnetic structures.

validate our theory and method with $RMnO_3$. These existing foundations enabled our current advances, and are instrumental in verifying the validity of our isomorphic theory and classification method.

The inversion symmetry breaking of the parent phases leads all $RMnO_3$ to exhibit SHG effects. The SHG effect of the A_1 phase belongs to the O-woP type, and the SHG effects of the other three phases fall into the BW-woP type. The even SHG tensors of the four magnetic phases possess the same characteristics, which are constrained by PG $G_0 = 6mm$. However, the odd SHG tensors differ for every magnetic phase, due to the different symmetry constraints as shown in Fig. 5b–e. The calculated nonzero SHG susceptibilities of $YMnO_3$ with the four magnetic structures are depicted in Fig. 5b–e, which are consistent with the symmetry analysis results (see Supplementary Table X) and previous studies[11,12,16,17,62–65]. The magnitude of the even SHG susceptibilities is almost one order of magnitude larger than those of odd parts in $RMnO_3$, as presented in Fig. 5b, which may be caused by the weak spin-orbit coupling (SOC) effect[24–26] in $YMnO_3$.

The in-plane even SHG components $\chi^{\text{even}}_{abc}(a,b,c \in \{x,y\})$ vanish in all magnetic phases due to the C_{2z} symmetry in $G_0 = 6mm$. However, the isomorphic groups G_1 of the B_1 and B_2 phases break the C_{2z} symmetry, leading to the nonzero in-plane odd SHG components. While the in-plane SHG components of the B_1 and B_2 phases are different because these are constrained by distinct symmetries ($G_1(B_1) = \bar{6}m2$ and $G_1(B_2) = \bar{6}2m$). Besides, the symmetry of the A_2 phase (MPG: $6m'm'$) permits the LMO effect, with the calculated anti-symmetry photoconductivity of $YMnO_3$ presented in Fig. 5c. Despite sharing the same crystal structure, the different magnetic structures lead to distinctive SHG and LMO features, as summarized in Supplementary Table X. Therefore, these fingerprints can be used to distinguish the magnetic structures and domains of $RMnO_3$ via the SHG[16–18,62–67] and LMO effects.

DISCUSSION

In magnetically ordered materials, the SHG susceptibility can be expressed as a Tailor series expression in terms of the magnetic order parameter $\mathbf{M}$[11] (such as the magnetic moment in a ferromagnet, the Néel vector in a collinear antiferromagnet and the chirality in a non-collinear antiferromagnet):

$$\chi^{(2)}_{ijk} = \chi^{(2)}_{ijk}(\mathbf{M}^0) + \chi^{(2)}_{ijk}(\mathbf{M}^1) + \chi^{(2)}_{ijk}(\mathbf{M}^2) + \cdots, \tag{5}$$

where $\chi^{(2)}_{ijk}(\mathbf{M}^0)$ is independent of magnetic order, corresponding to the SHG effect only contributed by crystallographic asymmetry. The odd-order Tailor expansion terms, including $\chi^{(2)}_{ijk}(\mathbf{M}^1), \chi^{(2)}_{ijk}(\mathbf{M}^3), \chi^{(2)}_{ijk}(\mathbf{M}^5), \cdots$ contribute to the odd SHG tensors (c-type). As stated in Ref. [12], the even-type SHG effect (i-type) refers to non-invariance when $\mathbf{M}$ is reversed, allowing the even-order magnetic coupling $(\chi^{(2)}_{ijk}(\mathbf{M}^2), \chi^{(2)}_{ijk}(\mathbf{M}^4), \chi^{(2)}_{ijk}(\mathbf{M}^6), \cdots)$ to contribute SHG effect. In the PT-wP type SHG effect, such as bilayer CrI_3[25,61], the lowest Tailor term is $\chi(\mathbf{M}^1)$, and only the odd-order terms exist. While for the G-wP type SHG effect, such as bulk VBr_2, the lowest Tailor term is $\chi(\mathbf{M}^2)$, however the zero-order $\chi(\mathbf{M}^0)$ and the linear-order term $\chi(\mathbf{M}^1)$ are forbidden by symmetry.

It is noted that our study is mainly focused on the SHG effect induced by the bulk electric dipole. The classification method can also be extended to the SHG effect arising from surface electric dipole provided that the surface crystal and magnetic structures are given. In centrosymmetric materials, the magnetic-dipole-type

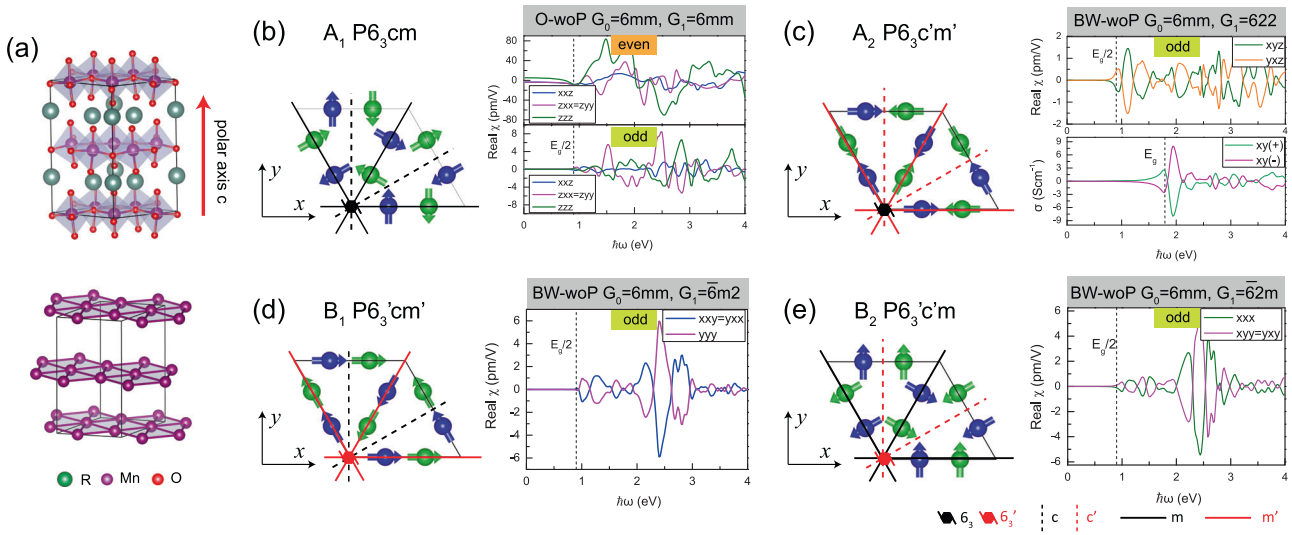

Fig. 5 Magnetic structures and SHG properties of $RMnO_3$ (R = Sc, Y, In, Dy, Ho, Er, Tm, Yb, and Lu) with different magnetic structures. **a** Crystal structure of $RMnO_3$. Magnetic structures of $RMnO_3$ with **b** A_1 ($P6_3cm$), **c** A_2 ($P6_3c'm'$), **d** B_1 ($P6'_3cm'$) and **e** B_2 ($P6'_3c'm$) phases. The blue and green balls in **b**–**e** mean the Mn^{3+} ions at different layers (top view). The right panels in **b**–**e** are the SHG susceptibilities of $YMnO_3$ with corresponding magnetic structures on the left. The lower panel of **c** is the calculated antisymmetric photoconductivity. The detailed magnetic and band structures are given in Supplementary Note 5.3.

and electric-quadrupole-type SHG are permitted by symmetry. For example, the SHG effect in Cr_2O_3[68] and monolayer CrSBr[9]. Even thorough, there are prior works on magnetic-dipole SHG effect by Hanamura and Valentí et al.[51,52,69–71] using semi-classical methods to treat the magnetic-dipole moment operator, evaluating the magnetic-dipole-type and electric-quadrupole-type SHG effect in first-principles calculations remain tough issues. Because it is very complicated to accurately treat the magnetic-dipole and electric-quadrupole operators, and capture their interplay with electric fields in density functional theory (DFT). Hence, the magnetic-dipole-type and electric-quadrupole-type SHG effects are not numerically studied in this work. However, we think our isomorphic group method can also be applied to investigate the characteristics of these two SHG effects, which need to be further studied.

According to the classification presented in Table 2, the physical mechanisms of the SHG effect can be classified into three main aspects: the even SHG effect arising from crystal asymmetry, the even SHG effect caused by magnetic structure, and the odd SHG effect caused by magnetic structure. As summarized in Table 3, we will compare them in the following. Specifically, the magnetic structure can contribute to both the odd and even SHG tensors, which vanish when the magnetic order or SOC effects in the coplanar magnetically ordered materials disappear. In this case, only the even SHG tensors contributed by the crystal structure asymmetry survive. For semiconducting magnetically ordered materials, χ^{even} is non-zero, while χ^{odd} disappears in the zero frequency limit ($\omega \to 0$, see Supplementary Note 5.5 for detail). The conditions to obverse them individually are in non-magnetically ordered materials, G-wP type and PT-wP type magnetically ordered materials, respectively, as listed in Table 3. The three parts in Table 3 can coexist in magnetically ordered materials whose parent phases have no inversion symmetry, corresponding to BW-woP and O-woP types SHG effect. It should be noted that the seven types of SHG identified in our work require further experimental verification. Therefore, we encourage researchers to perform experiments and simulations to validate our proposed classification and uncover distinctive SHG characteristics in magnetically ordered materials.

In conclusion, the classification of the SHG effect in magnetically ordered materials is performed to reveal the symmetries and physical mechanisms. Specifically, the isomorphic group method is utilized to study the SHG tensor for every MPG. This method simplifies the SHG tensor characteristics under MPGs into nonmagnetic PGs, revealing the symmetry rules governing the SHG effect. Furthermore, a tensor dictionary containing SHG and LMO effects is created, serving as guidance for experimentally probing magnetic structures. Subsequently, the SHG effect is classified into seven distinct types based on the symmetries of the magnetic and parent crystal structures. Assisted by this classification, a database cataloging SHG and LMO effects of materials in MANGDATA is established. The proposed classification method builds a close relationship between the SHG effect and magnetic structures and enhances the understanding of the SHG effect in magnetically ordered materials.

METHODS

First-principles calculations

The first-principles calculations based on DFT are performed using the VASP software package[72,73]. Moreover, the general gradient approximation (GGA) according to the Perdew-Burke-Ernzerhof (PBE) functional is employed, and the spin-orbit coupling effects are considered for all the materials. $U_{eff} = 3.0$ eV (5.0 eV) is set for V (Mn) atoms in VBr_2 ($YMnO_3$) calculations. The Bloch wave functions are iteratively transformed into maximally localized Wannier functions using the Wannier90 package[74,75]. The SHG susceptibilities and antisymmetric photoconductivities are calculated using our program WRFP (Wannier Response Function Package) based on the effective tight-binding (TB) Hamiltonian obtained by Wannier90.

Symmetries analysis of magnetically ordered materials

The symmetries of magnetically ordered materials are determined by the FINDSYM website[76], the and MPGs and MSGs are analyzed with the help of Bilbao Crystallographic Server[77]. The magnetic structures are visualized using VESTA software[78].

Table 3. Distinctive features of different physical mechanisms of SHG effect in magnetically ordered materials.

	Even from crystal asymmetry	Even from magnetic structure	Odd from the magnetic structure
Without magnetic order	✓	×	×
Without SOC effect[a]	✓	×	×
Zero frequency limit[b]	✓	✓	×
Reverse magnetic order	Invariant	Invariant	Reverse
Individually existing condition[c]	Non-magnetically ordered materials	G-wP	PT-wP

[a]For the coplanar magnetically ordered materials, see Supplementary Note 5.4 for more information.
[b]For semiconducting magnetically ordered materials, see Supplementary Note 5.5 for more information.
[c]"Individually existing condition" refers to the symmetry requirements to observe the SHG effect arising from crystal asymmetry, the even SHG effect caused by magnetic structure, and the odd SHG effect caused by magnetic structure, individually.

DATA AVAILABILITY

All data required to support the conclusions are presented in the paper. Additional data related to this paper can be requested from the authors.

Received: 6 March 2023; Accepted: 11 October 2023;
Published online: 24 October 2023

REFERENCES

1. Žutić, I., Fabian, J. & Das Sarma, S. Spintronics: fundamentals and applications. *Rev. Mod. Phys.* **76**, 323 (2004).
2. Sinova, J., Valenzuela, S. O., Wunderlich, J., Back, C. H. & Jungwirth, T. Spin hall effects. *Rev. Mod. Phys.* **87**, 1213 (2015).
3. Baltz, V. et al. Antiferromagnetic spintronics. *Rev. Mod. Phys.* **90**, 015005 (2018).
4. Faraday, M. I. Experimental researches in electricity.—nineteenth series. *Philos. Trans. R. Soc. London* **136**, 1–20 (1846).
5. Kerr, J. Xliii. On rotation of the plane of polarization by reflection from the pole of a magnet. *Philos. Mag.* **3**, 321–343 (1877).
6. Sun, Z. et al. Giant nonreciprocal second-harmonic generation from antiferromagnetic bilayer cri3. *Nature* **572**, 497 (2019).
7. Chu, H. et al. Linear magnetoelectric phase in ultrathin mnps3 probed by optical second harmonic generation. *Phys. Rev. Lett.* **124**, 027601 (2020).
8. Ni, Z. et al. Imaging the néel vector switching in the monolayer antiferromagnet mnpse3 with strain-controlled ising order. *Nat. Nanotechnol.* **16**, 782 (2021).
9. Lee, K. et al. Magnetic order and symmetry in the 2d semiconductor crsbr. *Nano Lett.* **21**, 3511 (2021).
10. Ju, H. et al. Possible persistence of multiferroic order down to bilayer limit of van der waals material nii2. *Nano Lett.* **21**, 5126 (2021).
11. Fiebig, M. & Pisarev, R. V. Nonlinear optics—a powerful tool for the investigation of magnetic structures. *J. Magn. Magn. Mater.* **272-276**, e1607 (2004).
12. Fiebig, M., Pavlov, V. V. & Pisarev, R. V. Second-harmonic generation as a tool for studying electronic and magnetic structures of crystals: review. *J. Opt. Soc. Am. B: Opt. Phys.* **22**, 96 (2005).
13. Pisarev, R. V. Second harmonic generation spectroscopy in magnetic and multiferroic materials. *J. Lumin.* **133**, 169 (2013).
14. Cheong, S.-W., Fiebig, M., Wu, W., Chapon, L. & Kiryukhin, V. Seeing is believing: visualization of antiferromagnetic domains. *npj Quant. Mater.* **5**, 3 (2020).
15. Němec, P., Fiebig, M., Kampfrath, T. & Kimel, A. V. Antiferromagnetic opto-spintronics. *Nat. Phys.* **14**, 229 (2018).
16. Fiebig, M., Lottermoser, T., Fröhlich, D., Goltsev, A. V. & Pisarev, R. V. Observation of coupled magnetic and electric domains. *Nature* **419**, 818 (2002).
17. Lottermoser, T. et al. Magnetic phase control by an electric field. *Nature* **430**, 541 (2004).
18. Manz, S. et al. Reversible optical switching of antiferromagnetism in TbMnO3. *Nat. Photon.***10**, 653 (2016).
19. Yokota, H., Hayashida, T., Kitahara, D. & Kimura, T. Three-dimensional imaging of ferroaxial domains using circularly polarized second harmonic generation microscopy. *npj Quant. Mater.* **7**, 106 (2022).
20. Pershan, P. S. Nonlinear optical properties of solids: energy considerations. *Phys. Rev.* **130**, 919 (1963).
21. Reif, J., Zink, J. C., Schneider, C. M. & Kirschner, J. Effects of surface magnetism on optical second harmonic generation. *Phys. Rev. Lett.* **67**, 2878 (1991).
22. Kirilyuk, A. Nonlinear optics in application to magnetic surfaces and thin films. *J. Phys. D: Appl. Phys.* **35**, R189 (2002).
23. Morimoto, T. & Nagaosa, N. Topological nature of nonlinear optical effects in solids. *Sci. Adv.* **2**, e1501524 (2016).
24. Fei, R., Song, W. & Yang, L. Giant linearly-polarized photogalvanic effect and second harmonic generation in two-dimensional axion insulators. *Phys. Rev. B* **102**, 035440 (2020).
25. Song, W., Fei, R., Zhu, L. & Yang, L. Nonreciprocal second-harmonic generation in few-layer chromium triiodide. *Phys. Rev. B* **102**, 045411 (2020).
26. Chen, H. et al. Basic formulation and first-principles implementation of nonlinear magneto-optical effects. *Phys. Rev. B* **105**, 075123 (2022).
27. Birss, R. R. *Symmetry and Magnetism* (North-Holland Publishing Company, 1964).
28. Birss, R. R. Macroscopic symmetry in space-time. *Rep. Prog. Phys.* **26**, 307 (1963).
29. Gallego, S. V. et al. Magndata: towards a database of magnetic structures. i. the commensurate case. *J. Appl. Crystallogr.* **49**, 1750 (2016).
30. Litvin, S. Y. & Litvin, D. B. Rank 0, 1, 2 and 3 magnetic and non-magnetic physical-property tensors. *Acta Crystallogr. A* **47**, 290 (1991).
31. Gallego, S. V., Etxebarria, J., Elcoro, L., Tasci, E. S. & Perez-Mato, J. M. Automatic calculation of symmetry-adapted tensors in magnetic and non-magnetic materials: a new tool of the bilbao crystallographic server. *Acta Crystallogr. A Found. Adv.* **75**, 438 (2019).
32. Železný, J. et al. Spin-orbit torques in locally and globally noncentrosymmetric crystals: Antiferromagnets and ferromagnets. *Phys. Rev. B* **95**, 014403 (2017).
33. Litvin, D. B. *Magnetic Group Tables 1-, 2- and 3-Dimensional Magnetic Subperiodic Groups and Magnetic Space Groups* (Reviewed by the IUCr Commission on Magnetic Structures, 2013).
34. Bardley, C. J. & Cracknell, A. P. *The Mathematical Theory of Symmetry in Solids: Representation Theory for Point Groups and Space Groups* (Oxford University Press, 2010).
35. Tao, R. *Group Theory in Physics (in Chinese)* (Shanghai Scientific & Technical Publishers, 1986).
36. Boyd, R. W. *Nonlinear Optics* (Academic press, 2010).
37. Shi, S., Chen, G., Zhao, W. & Jifang, L. *Nonlinear Optics (in Chinese)* (Xidian University press, 2012).
38. Šmejkal, L., MacDonald, A. H., Sinova, J., Nakatsuji, S. & Jungwirth, T. Anomalous hall antiferromagnets. *Nat. Rev. Mater.* **7**, 482–496 (2022).
39. Šmejkal, L., González-Hernández, R., Jungwirth, T. & Sinova, J. Crystal time-reversal symmetry breaking and spontaneous hall effect in collinear antiferromagnets. *Sci. Adv.* **6**, eaaz8809 (2020).
40. Feng, Z. et al. An anomalous hall effect in altermagnetic ruthenium dioxide. *Nat. Electron.* **5**, 735–743 (2022).
41. Zhou, X., Feng, W., Yang, X., Guo, G.-Y. & Yao, Y. Crystal chirality magneto-optical effects in collinear antiferromagnets. *Phys. Rev. B* **104**, 024401 (2021).
42. Gonzalez Betancourt, R. D. et al. Spontaneous anomalous hall effect arising from an unconventional compensated magnetic phase in a semiconductor. *Phys. Rev. Lett.* **130**, 036702 (2023).
43. Feng, W., Guo, G.-Y., Zhou, J., Yao, Y. & Niu, Q. Large magneto-optical kerr effect in noncollinear antiferromagnetsmn3x(x=rh,ir,pt). *Phys. Rev. B* **92**, 144426 (2015).
44. Higo, T. et al. Large magneto-optical kerr effect and imaging of magnetic octupole domains in an antiferromagnetic metal. *Nat. Photon.* **12**, 73–78 (2018).
45. Balk, A. L. et al. Comparing the anomalous hall effect and the magneto-optical kerr effect through antiferromagnetic phase transitions in mn3sn. *Appl. Phys. Lett.* **114**, 032401 (2019).
46. Wu, M. et al. Magneto-optical kerr effect in a non-collinear antiferromagnet mn3ge. *Appl. Phys. Lett.* **116**, 8194 (2020).
47. Zhou, X. et al. Spin-order dependent anomalous hall effect and magneto-optical effect in the noncollinear antiferromagnets mn_3xN with $x =$ Ga, zn, ag, or ni. *Phys. Rev. B* **99**, 104428 (2019).

48. Feng, W. et al. Topological magneto-optical effects and their quantization in noncoplanar antiferromagnets. *Nat. Commun.* **11**, 118 (2020).
49. Krichevtsov, B. B., Pavlov, V. V., Pisarev, R. V. & Gridnev, V. N. Spontaneous nonreciprocal reflection of light from antiferromagnetic cr2o3. *J. Phys. Condens. Matter* **5**, 8233 (1993).
50. Hayashida, T., Arakawa, K., Oshima, T., Kimura, K. & Kimura, T. Observation of antiferromagnetic domains in cr2o3 using nonreciprocal optical effects. *Phys. Rev. Res.* **4**, 043063 (2022).
51. Muthukumar, V. N., Valentí, R. & Gros, C. Microscopic model of nonreciprocal optical effects in cr2o3. *Phys. Rev. Lett.* **75**, 2766 (1995).
52. Muthukumar, V. N., Valentí, R. & Gros, C. Theory of nonreciprocal optical effects in antiferromagnets: The case of cr2o3. *Phys. Rev. B* **54**, 433–440 (1996).
53. Ferre, J. & Gehring, G. A. Linear optical birefringence of magnetic crystals. *Rep. Prog. Phys.* **47**, 513–611 (1984).
54. Voigt, W. Doppelbrechung von im magnetfelde befindlichem natriumdampf in der rischtung normal zu den kraftlinien. *Mathematisch-Physikalische Klasse* **1898**, 355–359 (1898).
55. Cotton, A. & Mouton, H. Magneto-optical properties of colloids and heterogeneous liquids. *Ann. Chim. Phys.* **11**, 145–289 (1907).
56. Aizu, K. Possible species of ferromagnetic, ferroelectric, and ferroelastic crystals. *Phys. Rev. B* **2**, 754 (1970).
57. Gallego, S. V. et al. Magndata: towards a database of magnetic structures. ii. the incommensurate case. *J. Appl. Crystallogr.* **49**, 1941 (2016).
58. Nishi, M., Ito, Y., Kadowaki, H. & Hirakawa, K. Neutron polarization analysis study of vbr2. *J. Phys. Soc. Jpn.* **53**, 1214 (1984).
59. Kadowaki, H., Ubukoshi, K. & Hirakawa, K. Neutron scattering study of the triangular-lattice antiferromagnet vbr2. *J. Phys. Soc. Jpn.* **54**, 363 (1985).
60. McGuire, M. A. Crystal and magnetic structures in layered, transition metal dihalides and trihalides. *Crystals* **7**, 121 (2017).
61. Gudelli, V. K. & Guo, G.-Y. Antiferromagnetism-induced second-order nonlinear optical responses of centrosymmetric bilayer cri3. *Chin. J. Phys.* **68**, 896 (2020).
62. Fiebig, M. et al. Determination of the magnetic symmetry of hexagonal manganites by second harmonic generation. *Phys. Rev. Lett.* **84**, 5620–5623 (2000).
63. Fiebig, M., Lottermoser, T. & Pisarev, R. V. Spin-rotation phenomena and magnetic phase diagrams of hexagonal rmno3. *J. Appl. Phys.* **93**, 8194–8196 (2003).
64. Wehrenfennig, C. et al. Incompatible magnetic order in multiferroic hexagonal dymno$_3$. *Phys. Rev. B* **82**, 100414 (2010).
65. Meier, D. et al. Mutual induction of magnetic 3*d* and 4*f* order in multiferroic hexagonal ermno$_3$. *Phys. Rev. B* **86**, 184415 (2012).
66. Fröhlich, D., Leute, S., Pavlov, V. V. & Pisarev, R. V. Nonlinear optical spectroscopy of the two-order-parameter compound ymno3. *Phys. Rev. Lett.* **81**, 3239 (1998).
67. Qian, M., Dong, J. & Xing, D. Y. Optical properties of the ferroelectromagnet YMnO3 studied from first principles. *Phys. Rev. B* **63**, 155101 (2001).
68. Fiebig, M., Fröhlich, D., Krichevtsov, B. B. & Pisarev, R. V. Second harmonic generation and magnetic-dipole-electric-dipole interference in antiferromagnetic Cr2O3. *Phys. Rev. Lett.* **73**, 2127 (1994).
69. Tanabe, Y., Muto, M., Fiebig, M. & Hanamura, E. Interference of second harmonics due to electric and magnetic dipoles in antiferromagnetic cr$_2$o$_3$. *Phys. Rev. B* **58**, 8654–8666 (1998).
70. Muto, M., Tanabe, Y., Iizuka-Sakano, T. & Hanamura, E. Magnetoelectric and second-harmonic spectra in antiferromagnetic cr$_2$o$_3$. *Phys. Rev. B* **57**, 9586–9607 (1998).
71. Hanmura, E. & Tanabe, Y. Nonlinear optical responses of antiferromagnetic insulators. *J. Nonlinear Opt. Phys.* **11**, 99–123 (2002).
72. Kresse, G. & Furthmüller, J. Efficient iterative schemes for ab initio total-energy calculations using a plane-wave basis set. *Phys. Rev. B* **54**, 11169 (1996).
73. Kresse, G. & Joubert, D. From ultrasoft pseudopotentials to the projector augmented-wave method. *Phys. Rev. B* **59**, 1758 (1999).
74. Mostofi, A. A. et al. wannier90: A tool for obtaining maximally-localised wannier functions. *Comput. Phys. Commun.* **178**, 685 (2008).
75. Mostofi, A. A. et al. An updated version of wannier90: A tool for obtaining maximally-localised wannier functions. *Comput. Phys. Commun.* **185**, 2309 (2014).
76. Stokes, H. T. & Hatch, D. M. Findsym: program for identifying the space-group symmetry of a crystal. *J. Appl. Crystallogr.* **38**, 237 (2005).
77. Gallego, S. V., Tasci, E. S., de la Flor, G., Perez-Mato, J. M. & Aroyo, M. I. Magnetic symmetry in the bilbao crystallographic server: a computer program to provide systematic absences of magnetic neutron diffraction. *J. Appl. Crystallogr.* **45**, 1236 (2012).
78. Momma, K. & Izumi, F. Vesta 3 for three-dimensional visualization of crystal, volumetric and morphology data. *J. Appl. Crystallogr.* **44**, 1272 (2011).

ACKNOWLEDGEMENTS

The authors acknowledge the High-performance Computing Platform of Anhui University for providing computing resources. We thank Haowei Chen (Tsinghua University), Shu-Hui Zhang (BUCT), Bo-Lin Li (HFIPS), Yang Gao (USTC), Yang Gao (AUST), Chong Wang (CMU), Jian Zhou (Xi'an Jiaotong University), Jiang Zeng (Hunan University), Kai Huang (UNL), Weikang Wu (Shandong University), and Y. J. Jin (Nanyang Technological University) for their useful discussions. This work is supported by the National Key R&D Program of China (Grants No. 2022YFA1403700), the National Natural Science Foundation of China under No. 12204009, 12204003, 11947212, 11904001, Natural Science Foundation of Anhui Province under No. 2208085QA08 and 2008085QA29, in part by the Joint Funds of the National Natural Science Foundation of China and the Chinese Academy of Sciences Large-Scale Scientific Facility under Grant No. U1932156. R.C.X. would like to express his gratitude to his grandmother, who sadly passed away recently, for raising and caring for him throughout his childhood.

AUTHOR CONTRIBUTIONS

R.-C.X. conceived the project with H.L. and H.J.. R.-C.X. edited the code and performed the symmetry analysis and first-principles calculations. R.-C.X., H.J., and H.L. discussed the results and the writing. The manuscript was written through the contributions of all authors. All authors have approved the final version of the manuscript.

COMPETING INTERESTS

The authors declare no competing interests.

ADDITIONAL INFORMATION

Supplementary information The online version contains supplementary material available at https://doi.org/10.1038/s41535-023-00594-3.

Correspondence and requests for materials should be addressed to Rui-Chun Xiao, Hua Jiang or Hui Li.